Volume 1 | Number 1 | Jan 2013 | Pages 1–100

Dalton Transactions

An international journal of inorganic chemistry
www.rsc.org/dalton

ROYAL SOCIETY OF CHEMISTRY

This is an *Accepted Manuscript*, which has been through the Royal Society of Chemistry peer review process and has been accepted for publication.

Accepted Manuscripts are published online shortly after acceptance, before technical editing, formatting and proof reading. Using this free service, authors can make their results available to the community, in citable form, before we publish the edited article. We will replace this *Accepted Manuscript* with the edited and formatted *Advance Article* as soon as it is available.

You can find more information about *Accepted Manuscripts* in the **Information for Authors**.

Please note that technical editing may introduce minor changes to the text and/or graphics, which may alter content. The journal's standard **Terms & Conditions** and the **Ethical guidelines** still apply. In no event shall the Royal Society of Chemistry be held responsible for any errors or omissions in this *Accepted Manuscript* or any consequences arising from the use of any information it contains.

Graphic Abstract

Solvents dependent reactivities of di-, tetra- and hexanuclear manganese complexes: syntheses, structures and magnetic properties

Hua Yang,[a] Fan Cao,[b] Dacheng Li,[a] Suyuan Zeng,[a] You Song,*[b] and Jianmin Dou*[a]

An unusual solvent effect on the syntheses of Di-, tetra- and hexanuclear manganese complexes has been exhibited. Complex **5** displayed the first stacked, off-set 8-MC-3 azametallacrown, and magnetic measurements showed slow magnetic relaxation with $S = 4$ ground state as well as field induced magnetization saturation.

Dalton Transactions
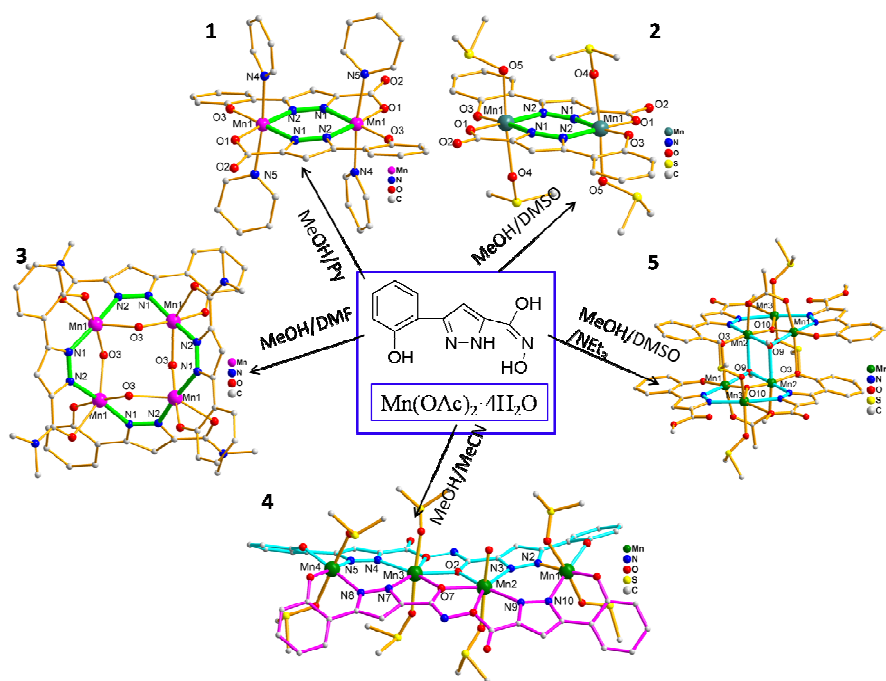
ARTICLE TYPE

Solvents dependent reactivities of di-, tetra- and hexanuclear manganese complexes: syntheses, structures and magnetic properties

Hua Yang,[a] Fan Cao,[b] Dacheng Li,[a] Suyuan Zeng,[a] You Song,*[b] and Jianmin Dou*[a]

5

An unusual solvent effect on the syntheses of five manganese complexes $[Mn_2(L_1)_2(Py)_4]$(**1**), $[Mn_2(L_1)_2(DMSO)_4]$(**2**), $[Mn_4(L_2)_4(OH)_4]$(**3**), $[Mn_4(L_3)_2(DMSO)_7(H_2O)]$(**4**), and $[Mn_6O_2(L_4)_4(OAc)_2(OMe)_2(DMSO)_4]\cdot MeOH]$ (**5**), (H_3L_1 = 5-(2-oxyphenyl)-pyrazole-3-carboxylic acid; H_2L_2 = 5-(2-oxyphenyl)-pyrazole-3-carboxylic acid amide; H_4L_3 = di-[5-(2-oxyphenyl)-pyrazole]-3-hydroxamic ether; and H_2L_4 = 5-(2-oxyphenyl)-pyrazole-3-carboxylic acid methyl ester) has been reported. Five complexes have been
10 characterized by X-ray single crystal diffraction, IR, element analysis, thermogravimetric analysis and UV-vis spectra. The analysis reveals that complexes **1** and **2** are isostructural with bimetallic six-membered ring and L_1 from the decomposition of the original H_4ppha (H_4ppha = 5-(2-hydroxyphenyl)-pyrazole-3-hydroxamic acid) ligand. Complexes **3** and **4** are two tetranuclear clusters, and **3** possesses an aza12-metallacrown-4 core with L_2 from the amide functionalization of the decomposition L_1; while **4** represents a novel linear $[Mn_4N_8O_2]$ core with L_3 from the condensation of L_1 and H_4ppha (H_4ppha = 5-(2-hydroxyphenyl)-pyrazole-3-hydroxamic acid).
15 Complex **5** is the first Mn_6 cluster linked by two stacked, off-set aza8-MC-3 subunits with [M−N−N−M−N−N−M−O] connectivity, and L_4 derived from the esterification of L_1. The magnetic behaviour of complexes **1−5** show the dominant antiferromagnetic interactions between mental centers, whereas complex **5** further reveals the coexisting of antiferromagnetic and ferromagnetic interactions, and slow magnetic relaxation at T < 6 K with S = 4 ground state as well as field induced magnetization saturation.

20 ## Introduction

Due to the intriguing architectures, catalyses and magnetic properties of the manganese coordination complexes, considerable effort has been devoted to their designs and syntheses from multidentate organic function ligands.[1] In view of
25 Mn^{III} ion having high anisotropy and Jahn-Teller elongation in the distorted octahedron coordinate environment, a survey reveals that a great of manganese complexes involving Mn^{III} ions usually represent different magnetic phenomena, such as single-molecule magnets (SMMs),[1a,2] single-chain magnets (SCMs),[3] and
30 magnetic frustration.[4] While these magnetic properties are relative to the metal ions and the topology structures of complexes. Thus, it is interesting to synthesize the attractive architectures with multiple high-spin Mn^{III} ions into one complex and explore the diverse magnetic properties.

35 A large number of manganese complexes focusing on the distinct structure and composition have been obtained through serendipity synthesis. The reason is that, in the experimental process, various factors, including reaction temperature, reaction period, concentration of the raw materials, metal-ligand ratio and
40 solution pH value, can affect the self-assembly of the resultant products. Among these parameters, solvents usually play a significant role in synthesizing coordination complexes.[5] Numerous reports have revealed that solvent effect on the crystal structures usually attributes to following factors, such as the
45 organic ligand solubility in solvents, solvent size and shape, solvent polarity, protic/aprotic behaviour and stoichiometric ratio of the mixed solvents.[5d,6] On the one hand, solvents as

coordination driven can assemble various structural topologies[7] and induce the single crystal structural transformation.[8] A study
50 showed that the more polar solvents seemed to participate in the self-assemble as coordination groups, whereas the less polar ones prefer to promote the formation of coordination complex with different structural aggregates.[9] On the other hand, solvents can give rise to the in-situ reaction of the original ligands, and the
55 resulting products can further function with metal ions to generate unprecedented structures.[10] Therefore, it is necessary to explore diverse structures in different solvents to obtain expectant complexes.

Metallacrowns (MCs) resemble organic crown with metal
60 atoms and nitrogen atoms replacing ring carbon atoms and exhibit −[M−N−O]− repeat unit,[11] while azametallacrowns (azaMCs), an extension class of metallacrowns, possess −[M−N−N]$_n$− ring cores.[11a,12] These cyclic complexes classes reported have been synthesized from hydroxamic acid,[11a,13]
65 oxime,[14] and hydrazine.[11a,15] A common feature is that these organic structures contain the N−O or N−N bridging linkers. We also reported a series of manganese complexes, some of which displayed metallazrown[16] or azametallacrown structures.[17] Interestingly, several cases involving pyrazolate organics with the
70 N−N bridging also exhibit azaMC structural types.[18] Thus, we expect to combine these two linkers (N−O and N−N) into one organic ligand aiming to obtain a series of novel coordination complexes. On the basis of the consideration, herein, we prepared a new pyrazolate-bridging hydroxamic acid ligand, H_4ppha
75 (H_4ppha = 5-(2-hydroxyphenyl)-pyrazole-3-hydroxamic acid), which possesses the rigid phenyl and pyrazolate rings, and flexible hydroxamic group. The reactions of H_4ppha with

manganese salts afforded five manganese complexes: two bimetallic six-membered ring complexes, one tetranuclear aza12-MC-4 complex, one linear [Mn$_4$N$_8$O$_2$] unit,[19] and a stacked, off-set aza8-MC-3 complex. All five complexes were characterized through single-crystal X-ray diffraction, IR, element analysis thermogravimetric analysis and UV-vis spectra. The structural analysis indicated the H$_4$ppha ligand underwent hydrolysis or concentration with the help of diverse solvents, and the resulting products further assembled to the different building block geometry. Moreover, the magnetic properties were discussed in detail.

Experimental section

Materials and physical methods

All chemicals used in the experiments are commercially available, and used as received without further purification. Elemental analyses of C, H and N were determined using an Elementar Vario EL analyzer. The IR (KBr pellet) spectra were measured on a Perkin-Elmer Spectrum with 400−4000 cm^{-1} region. Thermogravimetric experiments (TGA) were measured in a N$_2$ ambience with a heating range of 40−800℃ using a PerkinElmer TGA7 instrument. UV-vis NIR spectra were recorded on a Varian Cary 5000 spectrophotometer connected to a computer. The TGA curves and UV-visible spectra are shown in Fig. S1 and Fig. S2 (see Supporting Information†), respectively. Variable temperature magnetic susceptibility measurements were performed on a Quantum Design SQUID magnetometer MPMSXL in the temperature range of 1.8−300 K and in the magnetic field of 1 kOe. Measurements were carried out on polycrystalline samples of 23.6, 17.01, 21.23, 10.55 and 18.76 mg for **1−5,** respectively. Alternating current (ac) susceptibility measurements for complex **5** were carried out in the frequency range of 1−900 Hz with an oscillating field of 2 Oe.

X-ray Crystallography

Single-crystal X-ray diffraction data for complexes **1−5** were collected on a Bruker Smart CCD area-detector diffractometer with Mo Kα radiation (λ = 0.71073 Å) by ω-scan mode at room temperature. The program *SAINT* was used for integration of the diffraction profiles, and the semiempirical absorption corrections were applied using *SADABS*.[20,21] All of the structures were solved by direct methods using the *SHELXS* program of the *SHELXTL* package and refined by full-matrix least-squares methods with *SHELXL*.[22] Metal ions were located from the *E* maps, and the other non-H atoms were located in successive difference Fourier syntheses and refined with anisotropic thermal parameters on F^2.

Generally, C-bound H atoms were determined theoretically and refined with isotropic thermal parameters riding on their parents. H atoms of water and solvents were first located by difference Fourier *E* maps and then treated isotropically as riding. Crystallographic and structure refinement data were summarized in Table 1. The selected bond distances and angles were shown in Table S1 (see Supporting Information†). Crystallographic data for the structural analysis have been deposited with the Cambridge Crystallographic Data Center, CCDC reference number 983027 for **1**, 1003749 for **2**, 1003748 for **3**, 983029 for **4** and 1003747 for **5**.

Syntheses

H$_4$ppha ligand (L) (L = 5-(2-hydroxyphenyl)-pyrazole-3-hydroxamic acid)

1,3-Dioxo-1-(2-hydroxyphenyl)butyl methyl ester:[23] A solution of sodium ethoxide (prepared from sodium (7 g, 304 mmol)), acetophenone (26 g, 191 mmol) and diethyl oxalate (52 g, 191 mmol) in ethanolic (250 mL) was refluxed for 1 h. The resulting yellow solid was obtained by filtration, washed and dried at air. Then, the solid was dissolved in H$_2$O (200 mL), to which HCl (6 M) was added, and the brown precipitation was produced. The precipitation was collected after filtration and recrystallization. Yield: 28.69 g, 63.60%. **5-(2-oxyphenyl)-pyrazole-3-carboxylic acid methyl ester**:[23] Hydrazine monohydrate (4.064 g 40.6 mmol) was added to an ethanolic solution of 1,3-Dioxo-3-(2-hydroxyphenyl)butyl methyl ester (8 g, 33.9 mmol). The mixture was refluxed for 5 h at 90℃, then, cooled, filtered and washed to yield colorless product. Yield: 3.27 g, 41.63%. **H$_4$ppha**: The mixture of hydroxylamine hydrachloride (2.98 g, 42.9 mmol), 5-(2-oxyphenyl)-pyrazole-3-carboxylic acid methyl ester (1g, 42.9 mmol) and sodium hydroxide (5.15 g, 128.7 mmol) in ethanolic solution was stirred for 5 h at ice bath. The resulting product was filtered and dissolved in acid solution with pH = 3. The ochre product was obtained with the yield 0.42g, 44.85%.

[Mn$_2$(L$_1$)$_2$(Py)$_4$] (1)

The solution of Mn(OAc)$_2$·4H$_2$O (73.5 mg, 0.3 mmol) in MeOH (10 mL) was added to the solution of H$_4$ppha ligand (40.6 mg, 0.2 mmol) in pyridine (10 mL). The mixture was stirred for 5 h and the resulting dark brown solution was obtained. The solution was filtered and the filtration was allowed to evaporate slowly under ambient temperature for two weeks. X-ray quality black crystals were obtained and collected by filtration. Yield: 76% (based on Mn). Anal. Calcd for C$_{40}$H$_{30}$Mn$_2$N$_8$O$_6$ (%): C, 57.98; H, 3.65; O, 11.58; Found (%): C, 56.82; H, 3.04; O, 10.83. IR (KBr pellet, cm^{-1}): 3431m, 3119w, 3063w, 1656m, 1600m, 1559w, 1498w, 1488w, 1451m, 1397m, 1314m, 1294w, 1262m, 1213w, 1197w, 1159w, 1123w, 1068m, 1036w, 1017w, 860w, 830w, 780w, 762m, 691m, 644w, 587w, 542w, 487w, 469w, 400w.

[Mn$_2$(L$_1$)$_2$(DMSO)$_4$] (2)

Complex **2** was obtained by following the same procedure for **1** with the mixed solvents MeOH/DMSO (10 mL, v/v = 1:1) instead of pyridine. Yield: 56% (based on Mn). Calcd for C$_{28}$H$_{34}$Mn$_2$N$_4$O$_{10}$S$_4$ (%): C, 40.78; H, 4.15; O, 19.40; Found (%): C, 41.23; H, 3.94; O, 19.14. IR (KBr pellet, cm^{-1}): 3423s, 3119w, 3003w, 2915w, 1667s, 1598w, 1561w, 1498w, 1452m, 1396m, 1297m, 1259m, 1164w, 1131w, 1083w, 1037m, 1027m, 1000w, 946m, 863w, 836w, 794w, 767w, 684w, 643w, 565w, 538w, 453m.

[Mn$_4$(L$_2$)$_4$(OH)$_4$] (3)

Complex **3** was obtained by following the same procedure for **1** with the solvent DMF (10 mL) instead of pyridine. Yield: 11.5% (based on Mn). Anal. Calcd for C$_{48}$H$_{48}$Mn$_4$N$_{12}$O$_{12}$ (%): C, 47.85; H, 4.01; O, 15.94; Found (%): C, 47.16; H, 3.54; O, 16.32. IR (KBr pellet, cm^{-1}): 3417s, 3129w, 2925w, 1627s, 1563w, 1527w, 1503w, 1455m, 1394m, 1381w, 1300m, 1263m, 1212w, 1157w, 1125w, 1100w, 1080w, 1046w, 1035w, 986w, 866m, 840m, 784m,

754m, 690m, 673w, 647w, 634w, 602w, 567w, 537w, 477w, 454w.

[Mn$^{II}_2$Mn$^{III}_2$(L$_3$)$_2$(DMSO)$_7$(H$_2$O)] (4)[19]

The same procedure for **1** was performed in the mixed solvents MeCN/MeOH (10 mL, v/v = 2:1) replacing of pyridine, and the resulting precipitation was occurred. The precipitation was resolved in DMSO, and the suitable crystals were obtained for complex 4. Yield: 19% (based on Mn).

[Mn$_6$(μ_3-O)$_2$(L$_4$)$_4$(OAc)$_2$(OMe)$_2$(DMSO)$_4$]·MeOH] (5)

Complex **5** was obtained by following the same procedure for **1**

with the mixed solvents MeOH/DMSO (10 mL, v/v = 1:1) instead of pyridine in the presence of NEt$_3$. Yield: 57% (based on Mn). Anal. Calcd for C$_{60}$H$_{76}$Mn$_6$N$_8$O$_{26}$S (%): C, 42.72; H, 4.54; O, 24.66; Found (%): C, 42.05; H, 4.23; O, 25.22. IR (KBr pellet, cm^{-1}): 3434s, 3003w, 2951w, 1718m, 1700w, 1600w, 1548w, 1488m, 1450w, 1428w, 1409w, 1306w, 1294w, 1270w, 1246m, 1189w, 1146m, 1122w, 1077w, 1034m, 1015m, 960w, 864w, 853w, 807w, 775w, 749m, 675m, 656m, 586w, 534w, 486w, 430m.

Table 1. Crystal data and refinement information for complexes **1-3** and **5**.

Complex	1	2	3	4	5
Empirical	C$_{40}$H$_{30}$Mn$_2$N$_8$O$_6$	C$_{28}$H$_{34}$Mn$_2$N$_4$O$_{10}$S$_4$	C$_{48}$H$_{48}$Mn$_4$N$_{12}$O$_{12}$	C$_{54}$H$_{65}$Mn$_4$N$_{10}$O$_{18}$S$_7$	C$_{60}$H$_{76}$Mn$_6$N$_8$O$_{26}$S$_4$
M	828.6	824.71	1204.74	1586.34	1783.17
Crystal system	Triclinic	Monoclinic	Tetragonal	Monoclinic	Triclinic
Space group	$P\bar{1}$	P2(1)/c	I4(1)/a	$C2/c$	$P\bar{1}$
a/Å	9.4334(7)	9.2195(8)	22.683(2)	44.504(4)	11.2730(11)
b/Å	10.5064(10)	18.7801(19)	22.683(2)	14.6592(11)	12.4619(12)
c/Å	11.3707(12)	11.0378(12)	11.5196(9)	24.169(5)	13.9091(14)
α/°	64.1630(10)	90	90	90	108.769(2)
β/°	68.3970(10)	114.254(2)	90	103.539(2)	102.0300(10)
γ/°	70.361(2)	90	90	90	91.8560(10)
V/Å	922.05(15)	1742.4(30)	5926.9(9)	15330(2)	1799.0(3)
Z	1	2	4	8	1
D$_{calcd}$/g cm^{-3}	1.492	1.572	1.350	1.375	1.646
μ/mm^{-1}	0.745	1.023	0.897	0.900	1.222
F(000)	424	848	2464	6520	914
Crystal size/mm^3	0.45×0.38×0.33	0.43×0.40×0.35	0.13×010×0.08	0.33 × 0.31 × 0.13	0.45×0.32×0.27
Reflections collected/unique	4606 / 3192 [R(int)=0.0182]	8586 / 3059 [R(int)=0.0254]	12158 / 2618 [R(int)=0.1132]	38333 / 13513 [R(int) = 0.1341]	8733 / 6001 [R(int)=0.0996]
Goodness-of-fit on F^2	1.080	1.054	1.009	1.006	1.003
R_1 [I>2σ(I)]	0.0326	0.0555	0.0647	0.0782	0.1218
wR_2 (all data)	0.0900	0.1527	0.1582	0.1622	0.3872

Results and discussion

Synthesis

All five complexes were obtained from the reactions of Mn(OAc)$_2$·4H$_2$O and H$_4$ppha ligand in molar ratios of 1:1 in different solvents (MeOH, Py, DMF, DMSO and MeCN) in the presence/absence of NEt$_3$. The same crystallization process (slow evaporation) was used for all complexes. In the experimental process, the original H$_4$ppha ligand was hydrolyzed to 5-(2-oxyphenyl)-pyrazole-3-carboxylic acid (H$_3$L$_1$) in the mixed solvents of MeOH/Py or MeOH/DMSO. L$_1$ further underwent amidation and esterification with the help of DMF or MeOH to form 5-(2-oxyphenyl)-pyrazole-3-carboxylic acid amide (H$_2$L$_2$) and 5-(2-oxyphenyl)-pyrazole-3-carboxylic acid methyl ester (H$_2$L$_4$), respectively, or L$_1$ further condensed with H$_4$ppha to generate di-[5-(2-oxyphenyl)-pyrazole]-3-hydroxamic ether (H$_4$L$_3$). In the mixed solvents of MeOH/Py, complex **1** was obtained in the presence/absence of NEt$_3$. In the mixed solvents of MeOH/ DMSO, complex **2** was synthesized without any base,

while the existence of NEt$_3$ leaded to the formation of complex **5**. The plausible mechanism was depicted in Scheme S1†.

Crystal structures of [Mn$_2$(L$_1$)$_2$(Py)$_4$] (1) and [Mn$_2$(L$_1$)$_2$(DMSO)$_4$] (2)

Single-crystal X-ray diffraction analysis reveals that complexes **1** and **2** are isostructural and both feature the centro-symmetric neutral molecules [Mn$_2$(L$_1$)$_2$(Py)$_4$](**1**) and [Mn$_2$(L$_1$)$_2$(DMSO)$_4$](**2**). The molecular structure of complex **1** is presented in Fig. 1, and a full description of its structure is given as representative example. It crystallizes in triclinic space group $P\bar{1}$ and consists of two Mn^{III} ions, two L$_1^{3-}$ ligands and four coordinated pyridine molecules. Two Mn^{III} ions are bridged through couple N-N groups to form a bimetallic six-membered ring [Mn(1)-N(1)-N(2)-Mn(1')-N(1')-N(2')]. Each tetradentate L$_1^{3-}$ ligand chelates two metal centers in their bischelating fashion to show four five-membered and three six-membered rings in the equatorial plane. Thus, these multiple rings enforce structural stability. Each Mn^{III} ion exhibits six-coordinate, octahedral geometry with N$_4$O$_2$ donor sets from two L$_1^{3-}$ ligands and two pyridine molecules. Four pyridine molecules

occupy the axial positions with the average Mn-N distance of 2.365 Å, suggesting the Jahn-Tell elongation. In the structure, Mn1···Mn1' distance is 4.020 Å with Mn ion deviating from the $\{Mn_2N_4\}$ plane of 0.044 Å. The dihedral angle of the least-squares plane of the pyrazole ring relative to the Mn-N(pz)-N(pz)-Mn plane is 6.5°, while the dihedral angle between pyrazole ring and benzene ring is 13.25°, both of which indicate the twisting of L_1^{3-} ligand.

For complex **2**, four DMSO molecules replace four pyridine molecules in the axial positions, respectively. The separation distance of Mn1···Mn1' is 3.967 Å with Mn ion deviating from the $\{Mn_2N_4\}$ plane of 0.032 Å. The dihedral angle of the least-squares plane of the pyrazole ring relative to the Mn-N(pz)-N(pz)-Mn plane is 4.79°, while the dihedral angle between pyrazole ring and benzene ring is 6.65°. The comparison of the intermetallic distances and twisting of the ligand between complexes **1** and **2** suggests the ligand flexibility and the steric effect of the solvent molecules. The small intermetallic distances favourably allow for through-space electronic interactions and exchange through the bridging ligand.

Complexes **1** and **2** also represent the similar packing arrangements. A 3D network is formed through the interactions of the non-coordinating carboxylate O atoms, the coordinated pyridine H atoms and pyrazole H atoms among complex **1** (Fig. S3†, Table S2†), while a 3D network is only involved the supermolecular interactions of the non-coordinating carboxylate O atoms and pyrazole H atoms between complex **2** (Fig. S4†, Table S2†).
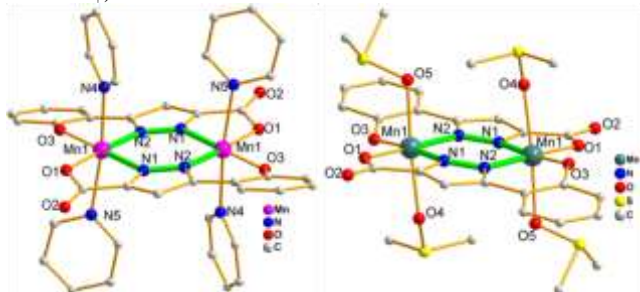

Fig. 1. Overall molecular structures of complexes **1** and **2**. Hydrogen atoms have been omitted for clarity.

Crystal structures of $[Mn_4(L_2)_4(OH)_4]$ (3) and $[Mn_4(L_3)_2(DMSO)_7(H_2O)]$ (4)

Complexes **3** and **4** are two tetranuclear complexes with different structural types. Complex **3** crystallizes in tetragonal space group $I4(1)/a$ and presents a classical aza12-MC-4 type (Fig. 2). The whole molecule possesses an ideal $S4$ symmetry, and four Mn ions are held together by four μ_2-OH$^-$, and four L_2^{2-}. In the structure, each μ_2-pyrazolyl unit spans per edge and points towards opposite sides. These alternating orientations in turning form a 12-MC-4 cyclic ring with $-[Mn-N-N]-$ repeat unit. Meanwhile, four μ_2-OH$^-$ also exhibit the similar bridging fashion with pyrazole motif to form a 8-membered cyclic ring with $[Mn-O]_n$ linkage, sharing metal centers with aza12-MC-4 ring.
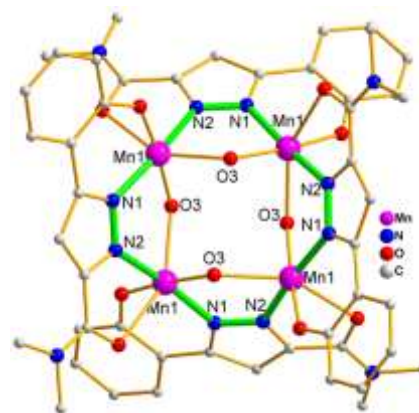

Fig. 2. Overall molecular structure of complex **3**. Hydrogen atoms have been omitted for clarity.

Each L_2^{2-} ligand connects two metal centers through pyrazole moiety and forms a six-membered and a five-membered chelatting rings with one phenoxide oxygen atom on one side and one acyl oxygen atom on the other side, respectively. Mn1 adopts six-coordination, distorted octahedral coordination geometry with N_2O_4 donor sets. The equatorial bond lengths range in 1.877(4)-2.012(5) Å and the axile bond lengths are 2.150(4) and 2.406(5) Å, indicating Jahn-Teller elongation. The combination of bond length, BVS calculation and the observed Jahn-Teller elongation axles reveals that four Mn ions are trivalent (Table S3†).

Furthermore, complex **3** also displays a 2×2 gridlike tetranuclear core with the adjacent Mn···Mn distance of 3.528 Å and the diagonal Mn···Mn distance of 4.941 Å. Two reported complexes with the different substituent groups in pyrazole were closely relating to **3**, one of which displays MeO$^-$ group instead of OH$^-$ in the skeleton.[18b,23] Besides, the supramolecular interactions between the terminal O2 atoms and amide methyl H atoms afford a 3D network (Fig. S5†, Table S2†).

The crystal structure of complex **4** is shown in Fig. 3. It was a mixed-valent tetranuclear complex $[Mn^{II}_2Mn^{III}_2(L_3)_2(DMSO)_7(H_2O)]$ with a novel linear $[Mn^{II}_2Mn^{III}_2N_8O_2]$ core. The molecular core consisted of two dimanganese-di-N-N-bridging subunits connected by two μ_2-hydroxamic-carboxylate oxygen and three contiguous rings form a (4, 2, 4) oxo-manganses-nitrogen linear arrangement.
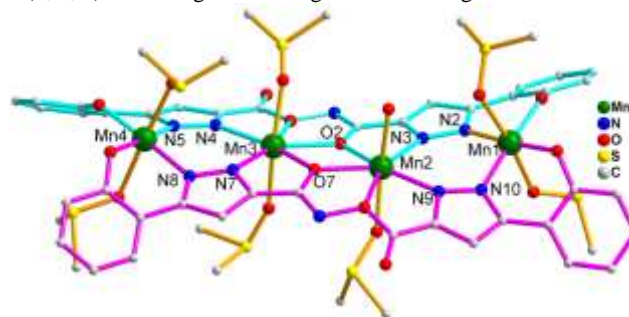

Fig. 3. Overall molecular structure of complex **4**. Hydrogen atoms have been omitted for clarity.

Crystal structure of $[Mn_6O_2(L_4)_4(OAc)_2(OMe)_2(DMSO)_4]$·MeOH (5)

Complex **5** is a hexanuclear complex with the formula as $[Mn_6(\mu_3\text{-}O)_2(L_4)_4(OAc)_2(OMe)_2(DMSO)_4]$·MeOH (**5**) (Fig. 4). It is located on an inversion center and has six Mn ions linked by

two μ_3-O^{2-}, four L_4^{2-} ligands, two μ_3-OMe^-, two μ_2-OAc^- groups and four coordinated DMSO molecules as well as one free MeOH. The arrangement of six Mn ions forms an expanded, stacked 8-MC-3 azametallacrowns with two parallel, off-set [Mn$_3$(μ_3-O^{2-})]
5 triangular subunits linked together through two μ_2-phenolate oxygen atoms and two μ_3-MeO^- groups. This complex also can be recognized as the first manganese stacked 8-MC-3 azametallacrown with the pyrazole-bridge, and each [Mn$_3$(μ_3-O^{2-})] subunit ring exhibits [Mn–N–N–Mn–N–N–Mn–O–] connectivity.
10 All six Mn ions adopt six-coordination, octahedral geometries with Jahn-Teller elongations in distorted octahedral geometry. In complex, four L_4^{2-} ligands display two coordination fashions: μ_2:η^2:η^1:η^1:η^1 and μ_2:η^1:η^1:η^1:η^1. Two OAc^- groups bridge Mn1 and Mn2 ions in their usual μ_2, syn-syn fashions. Four
15 crystallographically independent DMSO molecules complete the remaining coordination at Mn3 ion (and symmetry equivalent, s.e). The combination of bond lengths, charge balance and bond valence sum calculations reveals 2Mn^{II} (Mn3 and s.e) and 4Mn^{III} ions (Mn1, Mn2 and s.e) (Table S3†).
20 In each 8-MC-3 subunit, Mn$\cdots$Mn distances are 2.813, 3.4718, and 3.4718 Å for Mn(1)$\cdots$Mn(2), Mn(1)$\cdots$Mn(3) and Mn(2)$\cdots$Mn(3), respectively. The Mn-O(10) bond lengths are 1.808 Å for Mn(1), 1.796 Å for Mn(2) and 2.069 Å for Mn(3). The Mn-O(10)-Mn angles are 102.6° for Mn(1)-O(10)-Mn(2),
25 127.0° for Mn(1)-O(10)-Mn(3) and 127.0° for Mn(2)-O(10)-Mn(3). The μ_3-O^{2-} (10) ion deviates 0.173 Å from the Mn$_3$ (Mn1, Mn2 and Mn3) plane.

Although several stacked 9-MC-3 complexes from oxime ligands have been reported in Mn$_6$ clusters,[24] this complex
30 exhibits some obvious difference: (i) complex **5** possesses stacked, off-set 8-MC-3 triangular subunit with [Mn–N–N–Mn–N–N–Mn–O–] connectivity; (ii) the MeO^- group is involved in the formation of ring, and further bridge the third Mn ion of the adjacent triangular subunit; (iii) Mn1, Mn1' Mn2, Mn2' and their
35 bridging oxygen atoms (O3, O3', O9, O9', O10 and O10') form a fused defect-dicubane motif. Moreover, a 2D packing arrangement is formed via intermolecular C-H$\cdots$O supermolecular interactions (Fig. S6†), and the C-H$\cdots\pi$ interactions further afford structural stability (Table S2†).
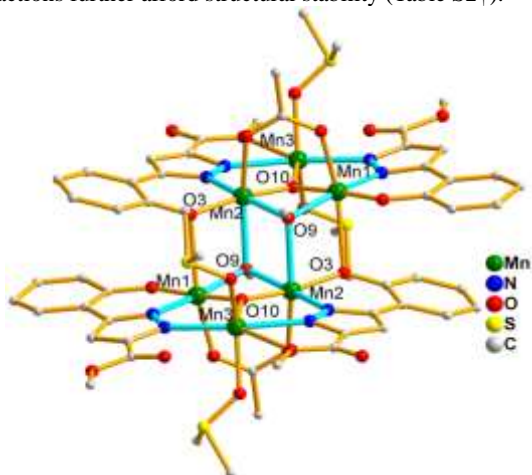

40 Fig. 4. Overall molecular structure of complex **5**. Hydrogen atoms and solvent molecule have been omitted.

Magnetic Properties

Mn^{III} ions are well known to possess four unpaired d electrons,
45 and can give rise to a large spin and molecular anisotropy according to Jahn-Teller effect in complexes. Solid-state, variable-temperature dc magnetic susceptibility data for complexes **1−5** were collected in the temperature range of 1.8−300 K on polycrystalline samples under an applied magnetic
50 field of 1 kOe. The collected data are plotted as $\chi_M T$ vs T curves in Fig. 5. The plots present similar near-plateaus above 50 K for complexes **1−4**. The $\chi_M T$ values of 5.6 (**1**), 6.03 (**2**), 11.9 (**3**), and 13.7 cm^3 K mol^{-1} (**4**) at 300K are close to the spin-only values, expected for magnetically isolated high-spin Mn^{III} and Mn^{II} ions
55 (6.00 (**1**), 6.00 (**2**), 12.00 (**3**), 14.75 cm^3 K mol^{-1} (**4**)). Upon cooling, the $\chi_M T$ products decreased to 0.32 (**1**), 0.81 (**2**), 1.75 (**3**) and 1.86 cm^3 mol^{-1} K (**4**) at 2 K. The decrease of $\chi_M T$ values indicates dominant antiferromagnetic coupling in the overall intramolecular exchange interactions.
60 For complexes **1** and **2**, the Hamiltonian can be written as $H = -2JS_1S_2$ (J is the interaction parameter). Thus, the eigenvalues can be given as $E(S) = -JS(S+1)$ with $S = S_1+S_2$. In view of all couplings, $E(S)$ can be given as follows:

$E(0) = 0$
65 $E(1) = -2J$
$E(2) = -6J$
$E(3) = -12J$
$E(4) = -20J$

For J < 0, which is usually the case, the ground state has the
70 smallest spin and the most excited state has the highest spin. Therefore, the magnetic susceptibility can be written as:

$$\chi = \frac{2Ng^2\beta^2}{\kappa T}\frac{e^{2x}+5e^{6x}+14e^{12x}+30e^{20x}}{1+3e^{2x}+5e^{6x}+7e^{12x}+9e^{20x}}$$

The fitting through the PHI[25] gives J = -1.02 cm^{-1}, g = 1.96 for **1** and J = -0.70 cm^{-1}, g = 2.0 for **2**. Moreover, the magnetic
75 susceptibility above 50 K can be fitted well by the Curie-Weiss law $\chi_M = C / (T - \theta)$, obtaining C = 5.73 cm^3 K mol^{-1}, θ = -4.36 K for **1** and C = 6.20 cm^3 K mol^{-1}, θ = -6.89 K for **2**. The negative θ values and exchange couplings again suggest the existence of antiferromagnetic interactions between the metal centers in
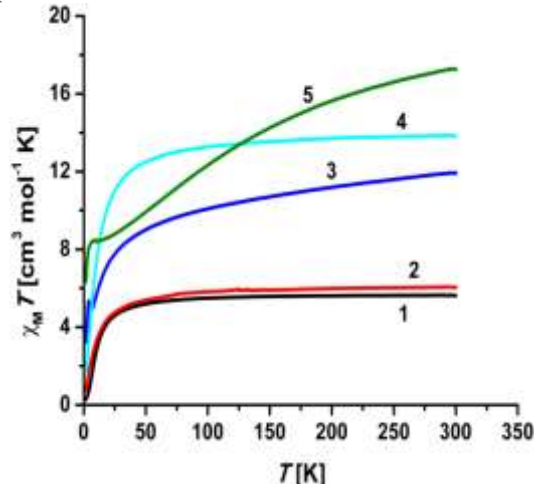80 complexes.

Fig. 5. The plots of $\chi_M T$ vs T for complexes **1–5**

For complex **3**, the decrease of $\chi_M T$ value also indicated the dominant antiferromagnetic interactions. The zero-field spin
85 Hamiltonian is given: $H = -2J(S_1S_2 + S_2S_3 + S_3S_4 + S_4S_1)$. The

relative energies of the low-lying states can be deduced (ESI†),[26] and all together there are 84 spin states. A good fitting[25] of the experimental data gave g = 1.84 and J = -0.34 cm^{-1}. While the fitting of Curie-Weiss law $\chi_M = C / (T - \theta)$ gave C = 12.85 cm^3 K
5 mol^{-1} and θ = -27.48 K. The negative J and θ values also again indicated the antiferromagnetic interactions. The presence of a maximum value in the $\chi_M T$ plot at low temperature maybe attributed to the paramagnetic impurity. In structure, all the edges were considered to be equivalent, and the exchange couplings
10 between neighboring manganese ions are equal. For J < 0, the adjacent local spins are not aligned parallel (Fig. S7†).

For complex **5**, the $\chi_M T$ product steadily decreased from 17.25 cm^3 K mol^{-1} at 300 K to reach 8.43 cm^3 K mol^{-1} with a small platform at 11 K. Upon cooling, the $\chi_M T$ value sharply dropped to
15 6.36 cm^3 K mol^{-1} at 1.8 K. The $\chi_M T$ value at room temperature is lower than the calculated spin-only value of 20.75 cm^3 K mol^{-1}, suggesting the dominant antiferromagnetic interactions between metal centers. The $\chi_M T$ value of 8.35 cm^3 K mol^{-1} at 6 K is consistent with S = 4 ground state. The decrease in $\chi_M T$ product at
20 low temperature may be relative with the zero-field splitting and/or Zeeman effect of the high-spin ground state, and/or intermolecular interactions. The exchange parameters between metal pairs can be given in Fig. 6. Many tries found that it was difficult for the fitting to obtain appropriate result owing to the
25 multiple exchange interactions. To simple the parameters, J_1 and J_4 can be combined into J. Then, the fitting[25] result of magnetic susceptibility gave J = 4.83 cm^{-1}, J_2 = -0.96 cm^{-1}, J_3 = -14.38 cm^{-1} and g = 1.98.
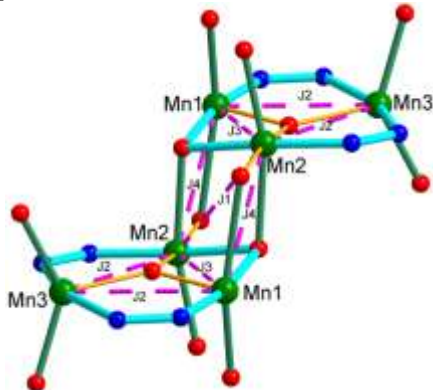

30   Fig. 6. The pairwise exchanging interaction in complex **5**.

To determine S = 4 ground state spin of complex **5**, the dc magnetization was investigated with magnetic field range of 1−70 kOe and temperature range of 1.8−20 K. The plots of $M − H$ are shown in Fig. S8†. The magnetization value rapidly increases at
35 the initial stage up to 20 kOe, and then steadily increases to 10.1 μ_B at 70 kOe at 1.8 K. The magnetization still slightly increases without saturation (Fig. S8† inset figure). The plots of $M − H/T$ are shown in Fig. S9†. The curves exhibit the nearly superimposition as decreasing magnetization, which indicates
40 only the ground state populates in the complex.

The ac susceptibility for complex **5** was measured to check for slow relaxation in the temperature range of 1.8−10 K with zero dc field using a 2.0 Oe ac field oscillating in the frequency range of 10−700 Hz. The in-phase ($\chi'_M T$) *vs* T and out-of-phase (χ''_M) *vs* T
45 plots have been shown in Fig. 7. As seen from the figure, there is a near-plateau in $\chi'_M T$ *vs* T plots above ~6 K with the $\chi'_M T$ value of 8.86 cm^3 K mol^{-1}. Upon decreasing, there is a steady decrease

in $\chi'_M T$ value and no frequency-dependent $\chi'_M T$ signals. Extrapolation of the plot from values above 6 K (to avoid the
50 effect of weak intermolecular interaction) to 0 K produces a value of 8.5 cm^3 K mol^{-1}, which is consistent with S = 4 ground state. Meanwhile, the ac susceptibility data reveals frequency-dependent out-of-phase (χ''_M) signals at temperature below 6 K, suggesting the superparamagnet-like slow relaxation of a SMM.
55 Despite the slow magnetic relaxation is observed at low temperatures, the maximum of χ''_M may be detected down to 2.0 K. Therefore, we could not go further in the analysis of the slow relaxation process (or the determination of the energy barrier and the time constant).
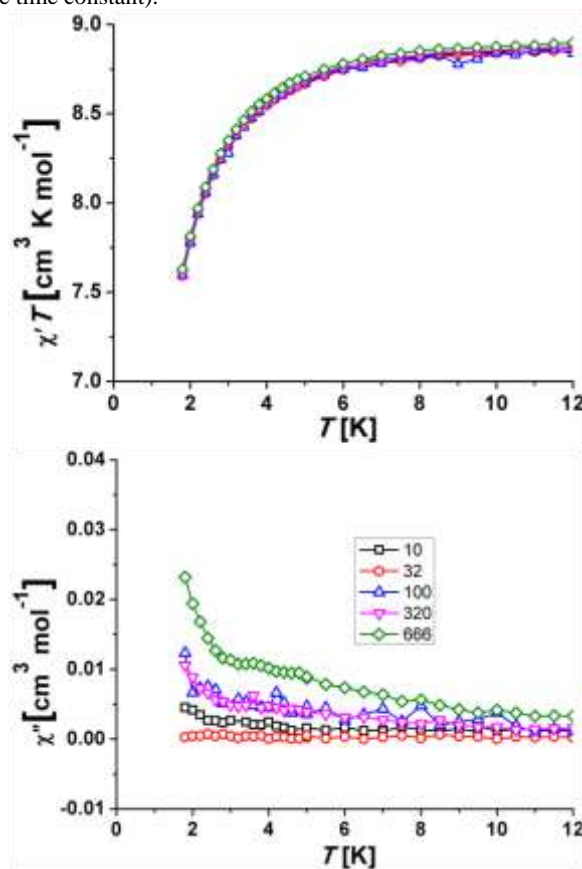

60
     Fig. 7. AC in-phase $\chi'_M T$ *vs* T plots (above) and out-of phase χ''_M *vs* T plots (below) in the temperature range of 1.8−12 K with zero dc field.

In order to confirm the energy barrier U_{eff} and τ_0, alternatively,
65 another method recently employed by Bartolomé et al., assume that there is only one characteristic relaxation process of the Debye type with one energy barrier and one time constant. With the assumption, the following relation is obtained:

$$\ln(\chi'' / \chi') = \ln(\omega\tau_0) + U_{eff} / \kappa T$$

70 which allows one to roughly evaluate U_{eff} and τ_0. Early, this method also has been applied to determine of the Mn_{12} acetate,[27] Dy_2 and Dy_3 complexes.[28] As shown in figure 8, by fitting the experimental χ''/χ' data, we extract an estimate of the activation energy of ~1.24 K and the characteristic time of 10^{-7}s. A more
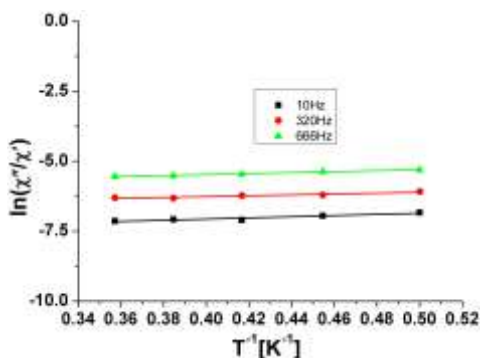75 precise result must wait for very low temperature measurements (T < 1 K) by using a micro-SQUID.

Fig. 8. Plot of natural logarithm of χ''/χ' vs $1/T$ for complex **5**. The solid line represents the fitting results over the range of 10 – 666 Hz. Slope corresponding to energy barrier $U_{\text{eff}} = 1.24$ K.

5 **Theoretical Model for 5.**

With all pairwise interactions, the complete spin Hamiltonian for **5** can be written as $H = -2J_1S_2S_2' - 2J_2(S_1S_3 + S_2S_3 + S_1'S_3' + S_2'S_3') - 2J_3(S_1S_2 + S_1'S_2') - 2J_4(S_1S_2' + S_1'S_2)$. The degeneracy and individual spin states of the hexanuclear $Mn^{III/II}$ complex will be large. It is
10 difficult to predict any particular ground state and not possible to use the Kambe vector-coupling approach owing to the difficulty in obtaining the absolute formula of energies states. A simple way is to explore the triangular aza8-MC-3 subunit in complex **5**. The pairwise interactions in each subunit system also can be seen
15 from figure 6. The Hamiltonian can be written as: $H = -2J_2(S_1S_3 + S_2S_3) - 2J_3S_1S_2$, $S_A = S_1 + S_2$, $S_T = S_A + S_3$. The eigenvalues can be given as $E(S_T, S_A) = -J_2[S_T(S_T+1) - S_A(S_A+1)] - J_3S_A(S_A+1)$. Figure 9 showed the energies of all 21 eigenstates ranging in S_T from 1/2 to 13/2 in units of J_2 as a function of the ratio J_3/J_2. For
20 both exchange interactions being antiferromagnetic, J_2 and J_3 are negative values. There are three different ground states (the ground state being defined by the bottom line for a given pointing point along the x axis), with S_T values being 1/2, 3/2, and 5/2. The PHI fitting[25] gives $J_3/J_2 = 15$. Thus, the aza8-MC-3 triangular
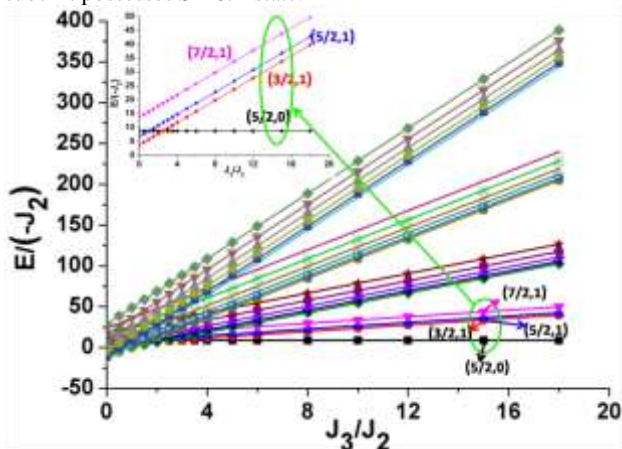25 subunit possesses $S = 5/2$ state.

Fig. 9. Plots of the eigenvales for a triangular array of $Mn^{III/II}$ ions in units of J_2. The states are labeled as (S_T, S_A). See text for details.

30 The local spin in such a triangular topology is represented schematically (Fig. S10†). The magnetic susceptibility of magnetic trimer in the low field was also given (ESI†). Due to the large Mn^{III}-Mn^{III} antiferromagnetic interactions, the local spins are aligned parallel along one of the two Mn^{II}-Mn^{III} edges.[26]

35 Consequentely, each triangular subunit only has $S = 5/2$ state. If each subunit can be considered as one paramagnetic ion, there are six low-lying spin states with the overall ground state ranging in 0−5. Both dc magnetic susceptibility and ac in-phase $\chi'_M T$ have provided enough evidence for the ground state spin $S = 4$. The
40 magnetization of 10.1 μ_B approaches saturation value, maybe, the field only gives the sum of two trinuclear units saturation values due to the very weak coupling interaction between two units.

Two triangular 8-MC-3 subunits are bridged through two MeO^- and two μ_2-phenolate oxygen atoms. The bond angles of
45 Mn1−O3/O9−Mn2 are 99.07° and 104.43°, and Mn2−O9−Mn2' is 101.93°. The exchange interactions involving the four linkers have two exchange parameters, namely J_1 and J_4. The fitting of magnetic susceptibility gave the total result of 4.83 cm^{-1}. Therefore, according to the above analysis, and bond lengths and
50 angular, we can deduced $J_1 > 0$, $J_4 < 0$ and $|J_1| > |J_4|$. Thus, the competitive result determined ferromagnetic interaction between two 8-MC-3 triangles. In other words, complex **5** represents an interesting example with antiferromagnetic and ferromagnetic interaction coexisting.

55 # Conclusion

Five Mn complexes have been obtained in different solvents. The structural analysis revealed the solvents have a significant effect on the syntheses and structures. The original ligand underwent hydrolysis, or the resultant further functioned with solvents
60 depending on the intrinsic polar, acid-base property of solvents or extra base. Complexes **1** and **2** are isostructural dinuclear complexes with centro-symmetric neutral molecules. Complexes **3** and **4** are two different tetranuclear clusters with **3** displaying aza12-MC-4 type possessing –[M–N–N]– repeat unit and **4**
65 exhibiting linear, novel $Mn_4N_8O_2$ core. Complex **5** is the first azametallacrown with stacked, off-set aza8-MC-3 structure exhibiting rare [Mn–N–N–Mn–N–N–Mn–O] connectivity. Magnetic susceptibility measurements show the complexes **1**–**4** behave dominant antiferromagnetic coupling between mental
70 centers, while **5** shows slow magnetic relaxation at temperature below 6 K with $S = 4$ ground state.

75 # Notes and references

[a] Shandong Provincial Key Laboratory of Chemical Energy Storage and Novel Cell Technology, School of Chemistry and Chemical Engineering, Liaocheng University, 252059 Liaocheng, People's Republic of China. Tel: 0635-8239298; E-mail: jmdou@lcu.edu.cn (J.D.)
80 *[b] State Key Laboratory of Coordination Chemistry, Collaborative Innovation Center of Advanced Microstructures, School of Chemistry and Chemical Engineering, Nanjing University, 210093 Nanjing, People's Republic of China. E-mail: yousong@nju.edu.cn (Y.S.)*

1 (a) G. E. Kostakis, A. M. Ako and A. K. Powell, *Chem. Soc. Rev*., 2010, **39**, 2238; (b) G. E. Kostakis, V. A. Blatov and D. M. Proserpio, *Dalton Trans*., 2012, **41**, 4634; (c) O. Roubeau and R. Clérac, Eur. J.
90 *Inorg. Chem*., 2008, **2008**, 4325; (d) E. Y. Tsui, J. S. Kanady and T. Agapie, *Inorg. Chem*., 2013, **52**, 13833.
2 (a) J. Martinez-Lillo, N. Dolan and E. K. Brechin, *Dalton Trans*., 2014, **43**, 4408; (b) D. P. Giannopoulos, A. Thuijs, W. Wernsdorfer, M.

Pilkington, G. Christou and T. C. Stamatatos, *Chem, Commun.*, 2014, **50**, 779; (c) J. Martinez-Lillo, N. Dolan and E. K. Brechin, *Dalton Trans.*, 2013, **42**, 12824; (d) E. Cremades, C. D. Pemmaraju, S. Sanvito and E. Ruiz, *Nanoscale*, 2013, **5**, 4751; (e) A. R. Farrel, J. A. Coome, M. R. Probert, A. E. Goeta, J. A. K. Howard, M-H. Lemée-Cailleau, S. Parsons and M. Murrie, *CrystEngComm.*, 2013, **15**, 3423; (f) P. L. Feng, C. C. Beedle, W. Wernsdorfer, C. Koo, M. Nakano, S. Hill and D. N. Hendrickson, *Inorg. Chem.*, 2007, **46**, 8126; (h) C. J. Milios, l. A. Gass, A. Vinslava, L. Budd, S. Parsons, W. Wernsdorfer, S. P. Perlepes, G. Christou and E. K. Brechin, *Inorg. Chem.*, 2007, **46**, 6215; (i) E. M. Rumberger, S. J. Shah, C. C. Beedle, L. N. Zakharov, A. L. Rheingold and D. N. Hendrickson, *Inorg. Chem.*, 2005, **44**, 2742; (j) T. N. Nguyen, W. Wernsdorfer, K. A. Abboud and F. Christou, *J. Am. Chem. Soc.*, 2011, **133**, 20688;

3   (a) P. L. Feng and D. N. Hendrickson, *Inorg. Chem.*, 2010, **49**, 6393; (b) K. Bernot, J. Luzon, R. Sessoli, A. Vindigni, J. Thion, S. Richeter, D. Leclercq, J. Larionova and A. van der Lee, *J. Am. Chem. Soc.*, 2008, **130**, 1619; (c) J. Yoo, W. Wernsdorfer, E. C. Yang, M. Nakano, A. L. Rheingold and D. N. Hendrickson, *Inorg. Chem.*, 2005, **44**, 3377; (d) W. X. Zhang, T. Shiga, H. Miyasaka and M. Yamashita, *J. Am. Chem. Soc.*, 2012, **134**, 6908; (e) N. E. Chakov, W. Wernsdorfer, K. A. Abboud and G. Christou, *Inorg. Chem.*, 2004, **43**, 5919; (f) X. Chen, S. Q. Wu, A. L. Cui and H. Z. Kou, *Chem. Commun.*, 2014, **50**, 2120; (g) G. Bhargavi, M. V. Rajasekharan, J.-P. Costes and J.-P. Tuchagues, *Dalton Trans.*, 2013, **42**, 8113; (h) C. I. Yang, Y.-J. Tsai, S.-P Hung, H.-L. Tsai and M. Nakano, *Chem. Commun.*, 2010, **46**, 5716; (i) M. Ding, B. Wang, Z. M. Wang, J. L. Zhang, O. Fuhr, D. Fenske and S. Gao, *Chem. A. Eur. J.*, 2012, **18**, 915; (j) X. Y. Song, P. P. Yang, X. L. Mei, L. C. Li and D. Z. Liao, *Eur. J. Inorg. Chem.*, 2010, **2010**, 1689.

4   (a) D. Liu, Q. Zhou, Y. Chen, F. Yang, Y. Yu, Z. Shi and S. H. Feng, *Dalton Trans.*, 2010, **39**, 5504; (b) A. G. Flamourakis, D. Tzimopoulos, M. Siczek, T. Lis, J. R. O'Brien, P. D. Akrivos and C. J. Milios, *Dalton Trans.*, 2011, **40**, 11371; (c) A. Escuer, B. Cordero, M. Font-Bardia, T. Calvet, O. Roubeau, S. J. Teat, S. Fedi and F. F. de Biani, *Dalton Trans.*, 2010, **39**, 4817.

5   (a) R. Díaz-Torres and S. Alvarez, *Dalton Trans.*, 2011, **40**, 10742; (b) X. C. Huang, J. P. Zhang, Y. Y. Lin and X. M. Chen; *Chem. Commun.*, 2005, **17**, 2232; (c) A. Y. Fu, Y.L. Jiang, Y. Y. Wang, X. N. Gao, G. P. Yang, L. Hou and Q. Z. Shi, *Inorg. Chem.*, 2010, **49**, 5495; (d) C. P. Li, J. M. Wu and M. Du, *Chem. Eur. J.*, 2012, **18**, 12437; (e) Y. F. Hou, B. Liu, K. F. Yue, C. S. Zhou, Y. M. Wang, N. Yan and Y. Y. Wang, *CrystEngComm.*, 2014, 10.1039/c4ce01359j; (f) J. X. Chen, J. K. Wang, J. Ulrich, A. X. Yin and L. Z. Xue, *Cryst. Growth Des.*, 2008, **8**, 1490; (g) R. D. Schmidt, C. A. Kent, J. J. Concepcion, W. B. Lin, T. J. Meyer and M. D. E. Forbes; *Dalton Trans.* 2014. DOI: 10.1039/c4dt01868k; (h) G. Z. Liu, S. H. Li; X. L. Li L. Y. Xin and L. Y. Wang; *CrystEngComm.*, 2013, **15**, 4571; (i) S. Zlatogorsky and M. J. Indrides, *Dalton Trans.*, 2012, **41**, 2685; (j) T. Baraille, S. Bracco, A. Comotti, F. Costantino, A. Guerri, A. Ienco and F. Marmottini; *CrystEngComm.*, 2012, **14**, 7170.

6   (a) C. P. Li and M. Du, *Chem. Commun.*, 2011, **47**, 5958; (b) L. Wen, P. Cheng and W. B. Lin, *Chem. Commun.*, 2012, **48**, 2846; (c) A.-Y. Fu, Y.-L. Jiang, Y.-Y. Wang, X.-N. Gao, G.-P. Yang, L. Hou and Q.-Z. Shi, *Inorg. Chem.*, 2010, **49**, 5495; (d) M. Feller, M. A. Iron, L. J. W. Shimon, Y. Diskin-Posner, G. Leitus and D. Milstein, *J. Am. Chem. Soc.*, 2008, **130**, 14374.

7   (a) M. Kawano and M. Fujita, *Coord. Chem. Rev.*, 2007, **251**, 2592; (b) J. Ramírez, A. M. Stadler, N. Kyritsakas and J. M. Lehn, *Chem. Commun.*, 2007, **3**, 237; (c) C. Tedesco, L. Reea, I. Immediata, C. Gaeta, M. Brunelli, M. Merlini, C. Meneghini, P. Pattison and P. Neri, *Cryst. Growth Des.*, 2010, **10**, 1527; (d) B. M. Kukovec, P. D. Vaz, M. J. Cahorda and Z. Popovic, *Cryst. Growth Des.*, 2010, **10**, 3685.

8   (a) H. X. Sun, W. L. Xie, S. H. Lv, Y. Xu, Y. Wu, Y. M. Zhou, Z. M. Ma, M. Fang and H. K. Liu, *Dalton Trans.*, 2012, **41**, 7590; (b) B. Liu, L. Y. Pang, L. Hou, Y. Y. Wang, Y. Zhang and Q. Z. Shi, *CrystEngComm.*, 2012, **14**, 6246; (c) S. K. Ghosh, W. Kaneko, D. Kiriya, M. Ohba, S. Kitagawa, *Angew. Chem. Int. Ed.*, 2008, **47**, 8843; (d) Y.-F. Han, W.-G. Jia, Y.-J. Lin and G.-X. Jin, *Angew. Chem.*, 2009, **121**, 6352;.

9   D. Krishna, A. Das and P. Dastidar, *Cryst. Growth Des.*, 2007, **7**, 2096.

10   M. F. Wang, X. J. Hong, Q. G. Zhan, H. G. Jin, Y. T. Liu, Z. P. Zheng, S. H. Xu and Y. P. Cai; *Dalton Trans.*, 2012, **41**, 11898;

11   (a) G. Mezei, C. M. Zaleski and V. L. Pecoraro, *Chem. Rev.*, 2007, **107**, 4933; (b) M. S. Lah and V. L. Pecoraro, *Comments Inorg. Chem.*, 1990, **11**, 59.

12   (a) B. Kwak, H. Rhee, S. Park, M. S. Lah, *Inorg. Chem.*, 1998, **37**, 3599; (b) S. Lin, S. X. Liu, Z. Chen, B. Z. Lin and S. Gao, *Inorg. Chem.*, 2004, **43**, 2222; (c) S. X. Liu, S. Lin, B. Z. Lin, C. C. Lin and J. Q. Huang, *Angew Chem. Int. Ed.*, 2001, **40**, 1084; (d) R. P. John, M. Park, D. Moon, K. Lee, S. Hong, Y. Zou, C. S. Hong and M. S. Lah, *J. Am. Chem. Soc.*, 2007, **129**, 14142.

13   (a) M. Tegoni and M. Remelli, *Coord. Chem. Rev.*, 2012, **256**, 289; (b) T. T. Boron III, J. W. Kampf and V. L. Pecoraro, *Inorg. Chem.*, 2010, **49**, 9104; (c) F. Dallavalle, M. Remelli, F. Sansone, D. Bacco and M. Tegoni, *Inorg. Chem.*, 2010, **49**, 1761; (d) A. B. Lago, J. Pasán, L. Cañadillas-Delgado, O. Fabelo, F. J. M. Casado, M. Julve, F. Lloret and C. Ruiz-Pérez, *New J. Chem.*, 2011, **35**, 1817; (e) J. Jankolovits, C.-S. Lim, G. Mezei, J. W. Kampf and V. L. Pecoraro, *Inorg. Chem.*, 2012, **51**, 4527; (f) A. V. Pavlishchuk, S. V. Kolotilov, M. Zeller, L. K. Thompson and A. W. Addison, *Inorg. Chem.*, 2013, **53**, 1320; (g) E. R. Trivedi, S. V. Eliseeva, J. Jankolovits, M. M. Olmstead, S. Peroud and V. L. Pecoraro, *J. Am. Chem. Soc.*, 2014, **136**, 1526.

14   (a) C. J. Milios, S. Piligkos and E. K. Brechin, *Dalton Trans.*, 2008, **14**, 1809; (b) A. Prescimone, C. J. Milios, S. Moggach, J. E. Warren, A. R. Lennie, J. Sanchez-Benitez, K. Kamenev, R. Bircher, M. Murrie, S. Parsons and E. K. Brechin, *Angew. Chem. Int. Ed.*, 2008, **47**, 2828; (c) C. I. Yang, W. Wernsdorfer, G.-H. Lee and H. L. Tsai, *J. Am. Chem. Soc.*, 2007, **129**, 456; (d) H. B. Xu, B. W. Wang, F. Pan, Z. M. Wang and S. Gao, *Angew. Chem. Int. Ed.* 2007, **46**, 7388; (e) C. J. Milios, R. Inglis, R. Bagai, W. Wernsdorfer, A. Collins, S. Moggach, S. Parsons, S. P. Perlepes, G. Christou and E. K. Brechin, *Chem. Commun.*, 2007, **33**, 3476; (f) H. L. Tsai, C. I. Yang, W. Wernsdorfer, S. H. Huang, S. Y. Jhan, M. H. Liu and G. H. Lee, *Inorg. Chem.*, 2012, **51**, 13171.

15   Y. T. Chen, H. Xu, J. M. Dou and D. C. Li, *Prog. Chem.*, 2008, **20**, 1666.

16   (a) X. J. Zhao, D. C. Li, Q. F. Zhang, D. Q. Wang and J. M. Dou, *Inorg. Chem. Commun.*, 2010, **13**, 346; (b) X. F. Shi, D. C. Li, S. N. Wang, S. Y. Zeng and D. Q. Wang, *J. Solid State Chem.*, 2010, **183**, 2144; (c) S. N. Wang, L. Q. Kong, H. Yang, Z. T. He, Z. Jiang, D. C. Li, S. Y. Zeng, M. J. Niu, Y. Song and J. M. Dou, *Inorg. Chem.*, 2011, **50**, 2705; (d) F. Cao, S. N. Wang, D. C. Li, S. Y. Zeng, M. J. Niu, Y. Song and J. M. Dou, *Inorg. Chem.*, 2013, **52**, 10747.

17   (a) J. M. Dou, M. L. Liu, D. C. Li and D. Q. Wang, *Eur. J. Inorg. Chem.*, 2006, **2006**, 4866; (b) Y. T. Chen, J. M. Dou, D. C. Li, S. N. Wang, and D. Q. Wang, *Inorg. Chem. Commun.*, 2010, **13**, 167.

18   (a) B. Schneider, S. Demeshko, S. Dechert and F. Meyer, *Angew. Chem. Int. Ed.*, 2010, **49**, 9274; (b) J. S. Costa, G. A. Craig, L. A. Barrios, O. Roubeau, E. Ruiz, S. Gómez-Coca, S.J. Teat and G. Aromí, *Chem. A. Eur. J.* 2011, **17**, 4960 ; (c) L. F. Jones, C. A. Kilner and M. A. Halcrow, *Chem. Eur. J.*, 2009, **15**, 4667; (d) J. J. Henkelis, L. F. Jones, M. P. de Miranda, C. A. Kilner and M. A. Halcrow, *Inorg. Chem.* 2010, **49**, 11127; (e) M. Veronelli, N. Kindermann, S. Dechert, S. Meyer and F. Meyer, *Inorg. Chem.*, 2014, **53**, 2333.

19   H. Yang, S. N. Wang, D. C. Li, S. Y. Zeng and J. M. Dou, *Inorg. Chem. Commun.*, 2014, **46**, 134.

20   SAINT v5.0-6.01; Bruker Analytical X-ray Systems Inc.:Madison, WI, 1998.

21   Sheldrick, G. M.SADABS; University of Göttingen: Göttingen, Germany.

22   SHELXTL v5.1, Bruker Analytical X-ray Systems Inc.: Madison, WI, 1999.

23   T. Matsumoto, T. Shiga, M. Noguchi, T. Onuki, G. N. Newton, N. Hoshino, M. Nakano and H. Oshio, *Inorg. Chem.*, 2010, **49**, 368.

24   (a) C. J. Milios, R. Inglis, A. Vinslava, R. Bagai, W. Wernsdorfer, S. Parsons, S. P. Perlepes, G. Christou and E. K. Brechin, *J. Am. Chem. Soc.*, 2007, **129**, 15205; (b) C. J. Milios, S. Piligkos and E. K. Brechin, *Dalton Trans.*, 2008, **14**, 1809; (c) A. G. Flamourakis, D. Tzimopoulos, M. Siczek, T. Lis, J. R. O'Brien, P. D. Akrivos and C. J. Milios, *Dalton Trans.*, 2011, **40**, 11371; (d) J. Martínez-Lillo, N. Dolan and E. K. Brechin, *Dalton Trans.*, 2014, **43**, 4408; (e) S. Sanz,

J. M. Frost, G. Lorusso, M. B. Pitak, S. J. Coles, G. S. Nichol and E. K. Brechin, *Dalton. Trans.,* 2014, **43**, 4622.

25 N. F. Chilton, R. P. Anderson, L. D. Turner, A. Soncini and K. S. Murray, *J. Comp. Chem*. 2013, **34**, 1164.

5 26 O. Kahn, Molecular Magnesim, VCH Publishers, Inc. NewYork, 1993, P 241.

27 F. Luis, J. Bartolome, J. F. Fernandez, J. Tejada, J. M. Hernandez, X. X. Zhang and R. Ziolo, *Phys. Rev. B*, 1997, **55**, 11448.

28 (a) Y.-N. Guo, X.-H. Chen. S. Xue and J-K. Tang, *Inorg. Chem*. 2011,
10   **50**, 9705; (b) S.-Y. Lin, L. Zhao, Y.-N. Guo, P. Zhang, Y. Guo and J.-K. Tang, *Inorg. Chem.* 2012, **51**, 10522.